

A single electric relaxation time in $\text{Ba}_{1-x}\text{Sr}_x\text{TiO}_3$ nanoparticles at low temperatures

Liyuan Zhang¹, Jun Zhou², Zhonglin Wang² and D Davidović¹

¹ School of Physics, Georgia Institute of Technology, Atlanta, GA 30332-0430, USA

² School of Materials Science and Engineering, Georgia Institute of Technology, Atlanta, GA 30332-0245, USA

E-mail: dragomir.davidovic@physics.gatech.edu

Received 20 November 2006, in final form 31 January 2007

Published 28 February 2007

Online at stacks.iop.org/Nano/18/135707

Abstract

It is shown that the dielectric response of $\text{Ba}_{0.77}\text{Sr}_{0.23}\text{TiO}_3$ nanoparticles at temperatures below 200 K has a frequency and temperature dependence in agreement with the Debye theory with a single relaxation time, which exhibits the Arrhenius law. By contrast, at temperatures above 210 K the dielectric response exhibits a broad range of relaxation times characteristic of relaxor-ferroelectrics. We suggest that the single relaxation time at low temperature originates from a frustration effect, in analogy with frustrated antiferromagnetism.

1. Introduction

Relaxor ferroelectrics are a class of disordered crystals with peculiar structure and properties [1]. For example, the typical dielectric response has a diffuse permittivity maximum which is frequency- and temperature-dependent. There are many theories proposed as an explanation for the unusual dielectric response of the materials such as non-interacting polar regions in the superparaelectric model [2], dipolar glass state [3], micro-domain state due to quenched random electric fields [4], random field theory based model [5] and Jonscher's many-body model [6].

Most recently the $\text{Ba}_{1-x}\text{Sr}_x\text{TiO}_3$ (BST) and BaTiO_3 (BTA) systems have received a lot of attention due to their promising dielectric properties when used as thin films [7–11] or nanowires [12, 13]: as examples, see the future generation of ultra-large-scale integrated dynamic random access memories (ULSI DRAMs) [14–16] and infrared detectors and filters [17]. In view of its high scientific and technologic importance, many measurements are made in a wide range of frequencies and temperatures, and for many types of impurity-induced relaxor ferroelectrics (such as BST and BCT) [18–24]. The measurements display the temperature and frequency dependence of the complex permittivity ($\epsilon^* = \epsilon' - i\epsilon''$) for thin films and bulk. Most experimental observations on bulk relaxor ferroelectrics are interpreted in terms of phenomenological

models based on a very broad spectral distribution of relaxation times.

The theories of BST bulk dielectric and ferroelectric properties are well developed [25, 26]. But nanometre-scale particles of these compounds are not well understood and they exhibit variation in their polarization behaviour with particle size [27–30], electric field and temperature [21]. Electric properties of these nanometre-scale particles are of fundamental interest for the physics of such dimensionally constrained microstructures. In addition, an understanding of their dielectric and ferroelectric properties is essential before they may be successfully integrated into commercial devices.

In this paper, we report measurements of the capacitance, which is equivalent to complex permittivity (ϵ^*), on the BST and BaTiO_3 (BTA) nanoparticles at frequencies between 10 Hz and 10^5 Hz, and in a temperature range of 4.2–340 K. We find a clear anomaly in both real and imaginary parts of permittivity at low temperatures. This anomaly has a frequency and temperature dependence that can be fitted by the Debye theory [31] with only one relaxation time (τ). The relaxation time exhibits the Arrhenius law instead of the Vogel–Fulcher law [32]. A single relaxation time at low temperatures is observed despite the fact that the room temperature permittivity exhibits a broad range of relaxation times typically found in relaxor ferroelectrics. We suggest that the low temperature anomaly in permittivity represents electric relaxation in a

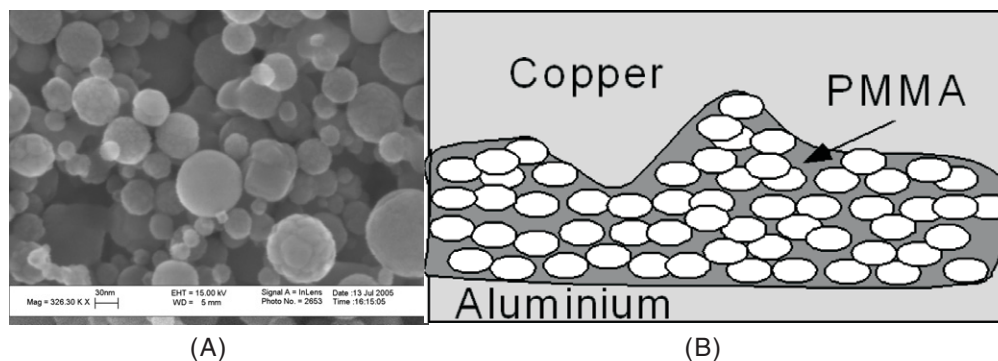


Figure 1. (A) SEM image of BST nanoparticles and (B) the sectional structure of the capacitor embedded with BST nanoparticles.

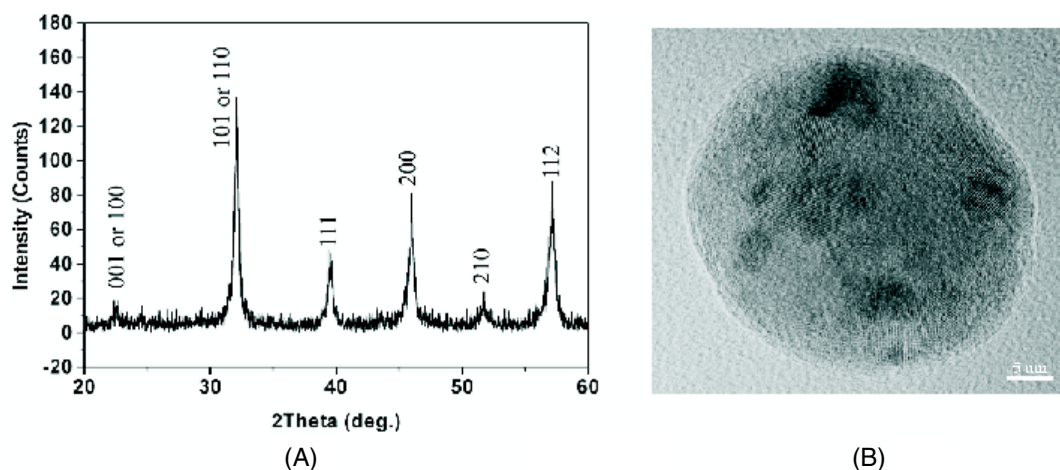


Figure 2. (A) The XRD pattern of BST nanoparticles and (B) the high-resolution TEM image of BST nanoparticles.

frustrated ferroelectric state of the nanometre-scale particles, analogous to frustrated antiferromagnets at low temperature.

2. Experimental procedure

BST ($\text{Ba}_{0.77}\text{Sr}_{0.23}\text{TiO}_3$) and BTA nanoparticles were manufactured by nGimat Company (<http://www.microcoating.com/nanotech/advantages.html>), using the combustion chemical vapour condensation (CCVD) technique, which works by decomposing metal-organic precursors in nanospray diffusion flames. Figure 1(A) is the image of these BST nanoparticles, obtained by a field emission scanning electron microscope (SEM). Most particles are spherical and the diameter varies from 5 to 100 nm. Most particles are not single crystals, and the crystallite size varies over a similar diameter range.

2.1. Characterization of the BST nanoparticles

The x-ray diffraction (XRD) pattern of the BST powder is shown in figure 2(A). All the peaks in the XRD pattern are attributed to the BST perovskite cube; the average crystallite size of the particles is 32 nm, which is estimated from the broadening of the (111) plane diffraction peak using the Scherrer equation. This size is similar to the average size of the BST particles observed from SEM and transmission electron

microscopy (TEM), figure 2(B). Figure 2(B) shows a high-resolution TEM image of BST particles, indicating that the BST particles are crystalline.

2.2. Device fabrication

Our samples are capacitors containing a dense array of nanoparticles in the insulation layer between the capacitor plates, sketched in figure 1(B). The capacitors are fabricated in two evaporation steps. First, an aluminium film with a basal area of $2 \times 20 \text{ mm}^2$ is thermally evaporated onto a SiO_2 substrate through a mask at 4×10^{-7} Torr pressure, and the Al film is then exposed to air. The nanoparticles are sonicated in methanol, which makes them well dispersed. Several drops of this methanol mixture are placed evenly over the Al film and then dried. This process creates a uniform deposit with thickness in the range of $\sim 100 \text{ nm}$ – $5 \mu\text{m}$, depending on the nanoparticle density in methanol. In our case, $5 \mu\text{m}$ thick nanoparticles are deposited and the thickness is measured by observing the cross section with an optical microscope. In the next step, the nanoparticles are spin-coated by a 400 nm thick layer of polymethylmethacrylate (PMMA) and baked out at 150°C to dry the PMMA. Finally, the nanoparticle film is covered with the top copper layer by thermal evaporation.

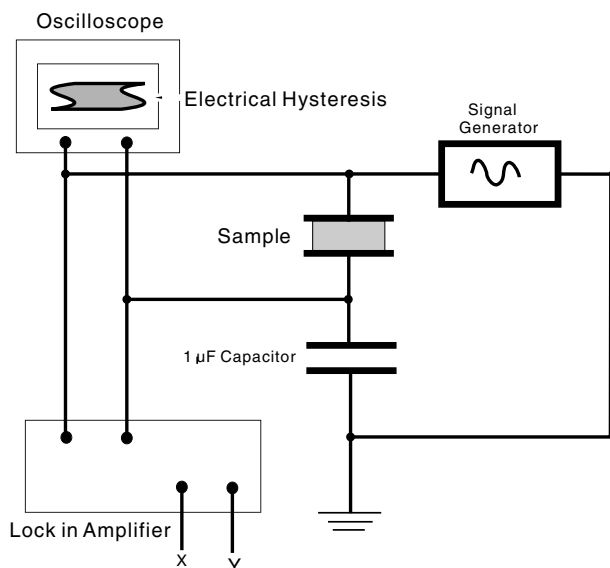


Figure 3. The measurement set-up of the Sawyer-Tower circuit.

3. Experimental results and discussion

Measurements are performed in the temperature range (4.2–340 K), using a liquid helium cryostat. Both complex capacitances and electrical hysteresis are measured by the Sawyer-Tower circuit [33], which is sketched in figure 3. The circuit is driven by a 0.1 V RMS sinusoidal signal, provided by a signal generator at frequencies (10, 10², 10³, 10⁴, 10⁵) Hz. The dielectric properties are commonly expressed as complex plane plots of permittivity, $\epsilon^* = \epsilon' - i\epsilon''$ and the equivalent complex capacitance given by $C^* = C' - iC''$. Using our sample dimensions, we can convert between ϵ^* and C^* as $\epsilon^* = (1.41 \times 10^{10} \text{ F}^{-1})C^*$.

The capacitance (C' and C'') versus temperature (T) in a typical sample is shown in figure 4. The data is obtained with an AC field corresponding to 0.1 V RMS and frequency 10³ Hz. In figures 4(A) and (B), the thick and the thin line correspond to increasing and decreasing temperatures, respectively. When the temperature increases from 4.2 K, initially both C' and C'' are constant and small. They are comparable to the stray capacitance of the leads. However, when the temperature reaches approximately 20 K, there is a significant and rapid increase in C' accompanied by a sharp peak in C'' . Later in the paper we will show that the C' increase and C'' peak are frequency-dependent. When the temperature is larger than about 30 K, both C' and C'' are constant again, until the temperature becomes close to 200 K. When the temperature increases above 200 K, both C' and C'' increase quickly and display a broad peak centred around 270 K. In addition, there are a few smaller peaks between 210 and 340 K.

When the temperature decreases from 340 to 4.2 K, C' and C'' exhibit hysteresis. The broad peak centred around 270 K has reduced amplitude upon reducing the temperature. However, at around 200 K, C' and C'' saturate and there is no more hysteresis below 200 K. That is, when the temperature is below 200 K, C' and C'' versus T is a single valued

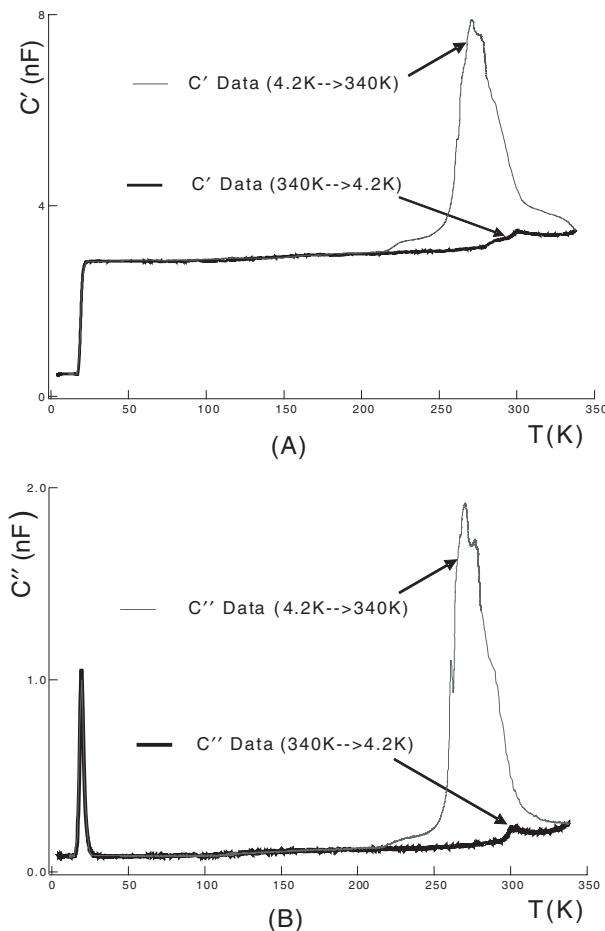


Figure 4. (A) Temperature dependence of C' and (B) C'' measured at 10³ Hz.

function of temperature. Only the temperature range above 210 K is characterized by hysteresis. The broad maximum in permittivity versus temperature above 210 K is a behaviour typical for relaxor ferroelectrics [2]. In this paper we focus on the low temperature properties of the nanoparticles ($T < 200$ K), where C' and C'' are single valued functions of temperature.

To determine the electric polarization versus applied electric field, we drive the capacitor by a triangle wave form with amplitude 3 V and frequency 10³ Hz. We use the Sawyer-Tower circuit (figure 3). Figure 5 displays the resulting polarization versus applied voltage. At temperatures close to the peak in C'' near 20 K and in the temperature range above 210 K, hysteresis is observed. P_r is the effective remanent polarization, E_c is the effective coercive field and P_s is the effective spontaneous polarization. P_r , E_c and P_s are not necessarily the same as the remanent polarization, the coercive field and the saturation polarization, respectively, because the hysteresis loop could originate from the time delay in the electric response. In particular, if the electric relaxation time is comparable to the period of the triangle wave, the hysteresis will occur because of the time delayed electric response of the sample.

In order to simulate the hysteresis loop, we assume a single relaxation time τ . The time variation of the dipole

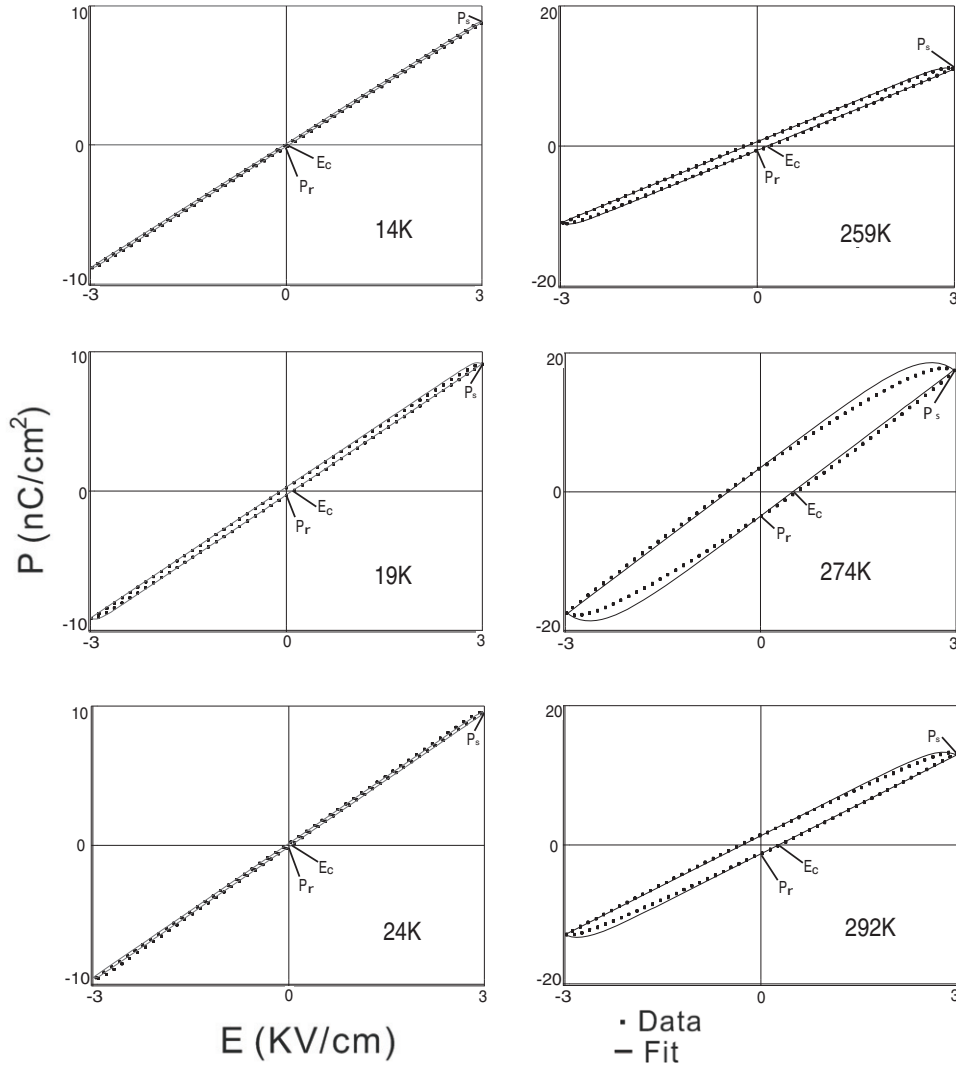


Figure 5. p versus ($E = V_{\text{applied}}/D$) hysteresis loops of experimental data (solid squares) at various temperatures and applied by a 10^3 Hz triangle wave. p versus E hysteresis loops (thin line) as calculated from equations (2) and (3) with the single relaxation time.

moment $P(t)$ for the permittivity in an alternating field $E = V_{\text{applied}}(t)/D$, where D is the thickness of the powder, is obtained from the linear differential equation:

$$\tau \frac{dP}{dt} + P = P_0 V_{\text{applied}}(t) / V_{\text{max}}, \quad (1)$$

where P_0 is the equilibrium dipole moment at voltage V_{max} and $V(t)$ is a triangle voltage wave with period $T = 2\pi/\omega$ and amplitude V_{max} . We take the Fourier transform of both sides in equation (1) and then obtain the $P(t)$:

$$P(t) = \sum_{n=1}^{\infty} \frac{8P_0(-1)^{n-1}}{\pi^2(2n-1)^2[1+(2n-1)^2\omega^2\tau^2]} \times [\sin[(2n-1)\omega t] - (2n-1)\omega\tau \cos[(2n-1)\omega t]] \quad (2)$$

$$V(t) = \sum_{n=1}^{\infty} \frac{8V_{\text{max}}(-1)^{n-1}}{\pi^2(2n-1)^2} \sin[(2n-1)\omega t] \quad (3)$$

where ω is the angular frequency of the applied field $V(t)$.

When $\omega t = 0$ and $\pi/2$, we have:

$$P(0) = \sum_{n=1}^{\infty} \frac{8P_0(-1)^n \omega \tau}{\pi^2(2n-1)[1+(2n-1)^2\omega^2\tau^2]} \quad (4)$$

$$P\left(\frac{\pi}{2\omega}\right) = \sum_{n=1}^{\infty} \frac{8P_0}{\pi^2(2n-1)^2[1+(2n-1)^2\omega^2\tau^2]} \quad (5)$$

Here $P(0)$ and $P(\pi/2\omega)$ correspond to P_r and P_s shown in figure 5, and we can obtain the values of relaxation time τ and dipole moment P_0 by solving equations (4) and (5). Then we obtain a single relaxation time model hysteresis loop $P(t)$ versus $E(t)$ using equations (2) and (3).

At temperature below 200 K, we found the hysteresis loops are fitted very well by the above model based on a single relaxation time. However, when the temperature is above 210 K, the experimental hysteresis shrinks compared with the curve fit that is calculated within a single relaxation time approximation. Thus, a single Debye process is a good fit at low temperatures, where the capacitance is a single valued

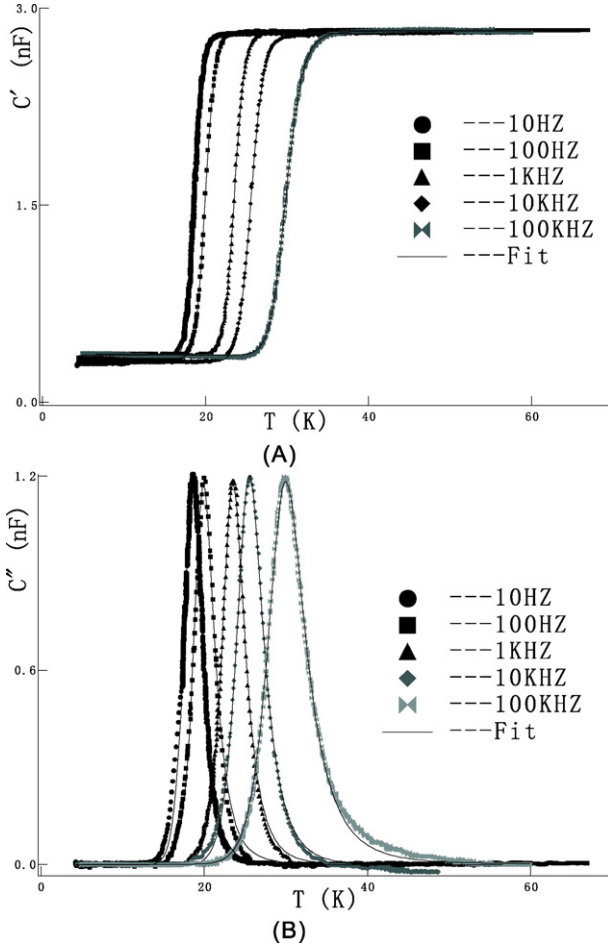


Figure 6. Temperature dependence at different frequencies of (A) the real parts C' and (B) the imaginary parts C'' .

function of temperature, but not above 200 K. The shrinkage of the data at 274 K compared to the single relaxation time model can be explained by a partial saturation of the electric polarization of the ferroelectric at large bias voltage.

The dielectric response of non-interacting dipoles should follow the classical frequency response. In a single relaxation time approximation equation (1) for a sinusoidal bias voltage leads to the complex dielectric permittivity:

$$\epsilon^*(\omega, \tau) = \epsilon_\infty + \frac{\epsilon_s + \epsilon_\infty}{1 + i\omega\tau} = \epsilon'(\omega, \tau) - i\epsilon''(\omega, \tau) \quad (6)$$

so the real and imaginary parts of the permittivity are:

$$\epsilon'(\omega, \tau) = \epsilon_\infty + \frac{(\epsilon_s - \epsilon_\infty)}{1 + \omega^2\tau^2} \quad (7)$$

$$\epsilon''(\omega, \tau) = \frac{(\epsilon_s - \epsilon_\infty)\omega\tau}{1 + \omega^2\tau^2} \quad (8)$$

where ϵ_s is the static dielectric constant ($\omega\tau \ll 1$) and ϵ_∞ is the high frequency dielectric constant where relaxation does not occur ($\omega\tau \gg 1$). From equations (7) and (8), we have:

$$\left(\epsilon'(\omega) - \frac{\epsilon_s + \epsilon_\infty}{2}\right)^2 + \epsilon''(\omega)^2 = \left(\frac{\epsilon_s - \epsilon_\infty}{2}\right)^2. \quad (9)$$

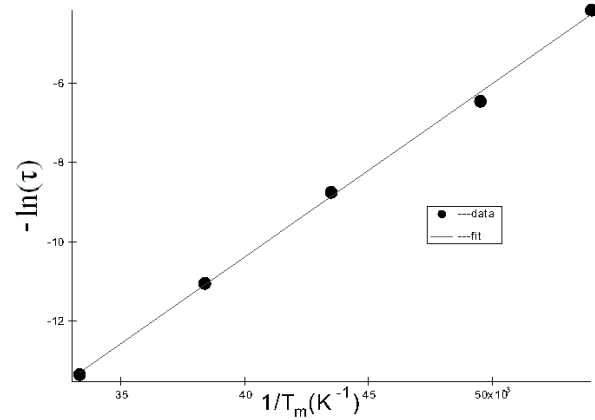


Figure 7. $-\ln(\tau)$ versus $1/T_m$ curve for BST (solid circles, the experiment data; thin line, the Arrhenius fits).

When $\omega\tau = 1$, we have:

$$\epsilon' = \frac{\epsilon_s + \epsilon_\infty}{2} \quad (10)$$

$$\epsilon'' = \epsilon''_{\max} = \left(\frac{\epsilon_s - \epsilon_\infty}{2}\right). \quad (11)$$

C'' versus T has a maximum when $\omega\tau = 1$. So, the relaxation time is $\tau = 1/\omega$ at temperature T where C'' has a maximum. Figure 6(B) displays C'' versus T at different frequencies of the sinusoidal bias voltage. The peak shift to lower temperatures with decreasing frequency demonstrates that τ increases as T decreases, as expected from the Arrhenius law for the relaxation time:

$$\tau = \tau_0 \exp\left(\frac{\Delta}{K_B T}\right), \quad (12)$$

where τ_0 is the inverse of the attempt frequency, $\tau_0 = 1/f_0$, and Δ is the activation energy to orient the dipoles.

The experimental data for the relaxation time versus T obtained from the maximum in C'' in figure 6(B) is shown in figure 7. The Arrhenius law is in quantitative agreement with our measurements. The activation energy and the attempt frequency are $\Delta = 37.8$ meV and $f_0 = 1.4$ THz, respectively.

The results of the measurements of the complex capacitance C' and C'' versus T are shown in figures 6(A) and (B). All data are measured at frequencies (10, 10^2 , 10^3 , 10^4 , 10^5) Hz and at a temperature range of 4.2–65 K. The markers indicate our experimental data, whereas the thin line is the curve fit based on equations (7) and (8). The relaxation time τ is based on the Arrhenius law (equation (12)), and the activation energy and the characteristic relaxation time τ_0 are set as free variable parameters in these fits. The following table is the result of the best fit value for the activation energy and the characteristic relaxation time.

Compared with the results fitted in figure 7, the fitting parameters' fluctuations in table 1 are large. Our temperature dependence measurements are done 'on the fly' and the sample is not in perfect thermal equilibrium with the thermometer, which is placed several centimetres away from the sample. We repeated the measurements of capacitance versus temperature, and found that the curves in figure 7 can shift by approximately

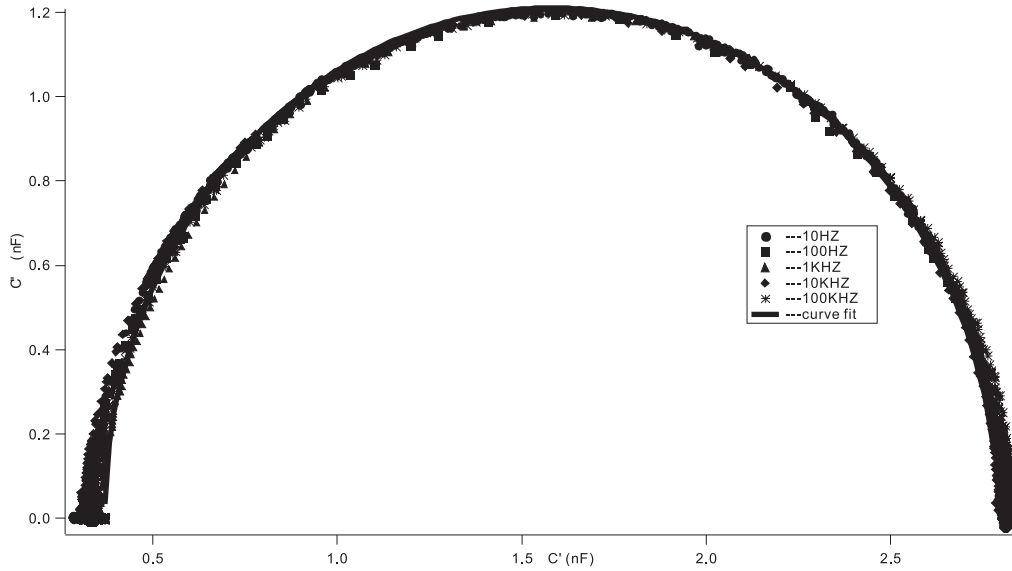


Figure 8. Cole–Cole plots (C' versus C'' is equivalent to ϵ' versus ϵ'') of the experimental data (markers) at the different frequencies (10, 10^2 , 10^3 , 10^4 , 10^5) Hz in the temperature range of 4.2–65 K and the curve fit (solid line) from equation (9).

Table 1. The single relaxation fitted by the Debye model and Arrhenius law.

ϵ^*	Parameters	10 Hz	10^2 Hz	10^3 Hz	10^4 Hz	10^5 Hz
Real part	$\frac{\Delta}{k_B}$ (K)	327.26	342.95	448.31	420.12	449.78
ϵ'	$\ln v_0$	19.687	20.397	23.407	21.941	21.714
	$\epsilon_s - \epsilon_\infty$ (nF)	2.5112	2.4979	2.4621	2.5038	2.4645
Image part	$\frac{\Delta}{k_B}$ (K)	351.33	355.53	445.5	446.74	441.67
ϵ''	$\ln v_0$	23.061	24.284	27.688	28.545	28.081
	$\epsilon_s - \epsilon_\infty$ (nF)	2.4167	2.3534	2.3529	2.4119	2.3683

2 K between different cool-downs. So the thermometer temperature is slightly different from the sample temperature when measuring on the fly. Nevertheless, excellent fits of the curve shapes provide adequate evidence for a single electric relaxation timescale in the sample.

The Cole–Cole plot, which displays out-of-phase capacitance versus in-phase capacitance, is shown in figure 8. All the experimental data are frequency-independent and located around a semicircle, as expected from equation (9). It is important to note that in the Cole–Cole plot the data fall on a semicircle even if the sample temperature is slightly different from the thermometer temperature. Thus, figure 8 proves that only one relaxation time is present, in contrast to two [34] or multi-relaxation time cases [35]. The data are fitted as shown by the solid black line based on equation (9). The fitting results are $C_s = 2.79$ nF, $C_\infty = 0.37$ nF.

We have repeated these measurements in about ten BST nanoparticle samples and found that our results are quantitatively reproducible. We have also done measurements in BTA nanoparticle samples, and found similar results for the electric polarization at low temperatures, with comparable relaxation time to that in BST nanoparticles.

4. Discussion

It is surprising that the electric relaxation in BST nanoparticle powders at low temperature has only one relaxation time,

because higher temperatures indicate relaxor ferroelectric behaviour with a broad distribution of relaxation times. The broad distribution is attributed to the variation in the local Néel temperature and variation in the local environments of the correlated electric dipoles [2]. At low temperatures, however, when the correlated dipoles are frozen into the ferroelectric state, our data shows that there remains a fraction of dipoles that are responsive to the changes in the applied electric field. These free dipoles are characterized by only one relaxation time. Since our sample has significant disorder, which is due to different crystallite size and local compositional variation, the relaxation process of these free dipoles must be insensitive to the disorder.

The attempt frequency $f_0 \sim 1$ THz is of the order of the optical phonon frequency, which suggests the free dipoles must be ions, not electrons. The energy barrier for tunnelling between sites (37.8 mV) is small compared to the ferroelectric free energy of the nanoparticles, which is proportional to the nanoparticle volume.

A single relaxation time shows that the activation energy does not vary among different ions and it is reproducible among samples. This shows that the activation energy must be set by the parameters of the crystal structure of BST, and not random defects.

There have been similar studies by Zhang *et al* [36–38] in large size grains, including studies of bulk ceramic $\text{Ba}_{0.7}\text{Sr}_{0.3}\text{TiO}_3$ (the composition similar to our sample) with

different grain size (1860, 1100, 370, 223 and 198 nm). They found some size effects on the dielectric properties with temperature changes from 10 to 400 K, generally that the dielectric constant and ferroelectric tendencies are suppressed with decreasing grain size. Their results showed non-Debye type response and non-Arrhenius form in relaxation time, which is totally different from our results below 200 K. In addition, the temperature dependence of the dielectric constant did not show any measurable thermal hysteresis with heating and cooling, whereas we find thermal hysteresis in our samples when the temperatures are above 210 K.

There are some other works [19, 20, 39–42] on size effects in BST which present the variations of the dielectric constant as a function of temperature. The cause of size effects in ferroelectrics is complicated, and it is often difficult to separate true size effects from the other factors that change with film thickness or particle size, such as film microstructure and defect chemistry or constraints such as electrode interaction and space charge layers and so on. None of these studies found a single relaxation time as in our paper.

In our samples, one possibility would be that the free dipoles are located on the nanoparticle surfaces, because the surface to volume ratio is large. But this explanation is problematic because different Ti ions on the surfaces would experience different crystal fields so one would expect a broad range of energy barriers Δ .

We suggest that these free dipoles are produced by some frustration effect, which prevents locking into the ferroelectric order. The electric frustration could occur because the ferroelectric state in nanometre-scale particles could be fundamentally different from ferroelectricity in bulk [43, 44]. Zero-dimensional ferroelectrics were shown to display phase transitions that are unknown in bulk [44] and we suspect that this could lead to a frustrated ferroelectric ground state, analogous to the frustration in frustrated antiferromagnets. The frustration would cause a fraction of the Ti ions to remain responsive to the applied electric field at temperatures much below the Néel temperature. Deeper theoretical investigation of the possible origins of frustrated behaviour is beyond the scope of the present paper.

5. Conclusion

The dielectric relaxation with a single relaxation time is observed in $\text{Ba}_{0.77}\text{Sr}_{0.23}\text{TiO}_3$ nanoparticles at low temperatures. The activation energy is 37.83 meV and the attempt frequency 1.4 THz. At high temperatures, the dielectric relaxation exhibits the features of the ferroelectric in the relaxor state. More theoretical work is desirable to understand electric relaxation in these nanoparticles at low temperatures.

Acknowledgments

We thank Andrew Hunt and Sundel Seth from nGimat for valuable discussions. This research has been supported by the David and Lucile Packard Foundation grant 2000-13874 and Nanoscience/Nanoengineering Research Program at Georgia-Tech.

References

- [1] Bokov A A and Ye Z G 2006 *J. Mater. Sci.* **41** 31–52
- [2] Cross L E 1987 *Ferroelectrics* **76** 241–67
- [3] Viehland D, Jang S J, Cross L E and Wuttig M 1990 *J. Appl. Phys.* **68** 2916–21
- [4] Westphal V, Kleemann W and Glinchuk M D 1992 *Phys. Rev. Lett.* **68** 847–50
- [5] Glinchuk M D and Farhi R 1996 *J. Phys.: Condens. Matter* **8** 6985–96
- [6] Jonscher A K 1981 *J. Mater. Sci.* **16** 2037–60
- [7] Junquera J and Ghosez P 2003 *Nature* **422** 506–9
- [8] Shaw T M, Trolier-McKinstry S and McIntyre P C 2000 *Annu. Rev. Mater. Sci.* **30** 263–98
- [9] Horikawa T, Mikami N, Makita T, Tanimura J, Kataoka M, Sato K and Nunoshita M 1993 *Japan. J. Appl. Phys.* **32** 4126–30
- [10] Cole M W, Joshi P C, Ervin M H, Wood M C and Pfeffer R L 2000 *Thin Solid Films* **374** 34–41
- [11] Kim W J, Chang W, Qadri S B, Pond J M, Kirchoefer S W, Chrisey D B and Horwitz J S 2000 *Appl. Phys. Lett.* **76** 1185–7
- [12] Yun W S, Urban J J, Gu Q and Park H 2002 *Nano Lett.* **2** 447–50
- [13] Geneste G, Bousquet E, Junquera J and Ghosez P 2006 *Appl. Phys. Lett.* **88** 112906
- [14] Scott J F and Dearaujo C A P 1989 *Science* **246** 1400–5
- [15] Dietz G W, Schumacher M, Waser R, Streiffer S K, Basceri C and Kingon A I 1997 *J. Appl. Phys.* **82** 2359–64
- [16] Auciello O, Scott J F and Ramesh R 1998 *Phys. Today* **51** 22–7
- [17] Padmini P, Taylor T R, Lefevre M J, Nagra A S, York R A and Speck J S 1999 *Appl. Phys. Lett.* **75** 3186–8
- [18] Bianchi U Dec J, Kleemann W and Bednorz J 1995 *Phys. Rev. B* **51** 8737–46
- [19] Wang R P, Inaguma Y and Itoh M 2001 *Mater. Res. Bull.* **36** 1693–701
- [20] Parker C B, Maria J P and Kingon A I 2002 *Appl. Phys. Lett.* **81** 340–2
- [21] Basceri C, Streiffer S K, Kingon A I and Waser R 1997 *J. Appl. Phys.* **82** 2497–504
- [22] Ang C, Yu Z and Jing Z 2000 *Phys. Rev. B* **61** 957–61
- [23] Lemanov V V, Smirnova E P, Surnikov P P and Tarakanov E A 1996 *Phys. Rev. B* **54** 3151–7
- [24] Lemanov V V, Sotnikov A V, Smirnova E P and Weihnacht M 2005 *J. Appl. Phys.* **98** 056102
- [25] Kingsmith R and Vanderbilt D 1994 *Phys. Rev. B* **49** 5828–44
- [26] Zhong W, Kingsmith R D and Vanderbilt D 1994 *Phys. Rev. Lett.* **72** 3618–21
- [27] Chattopadhyay S, Ayyub P, Palkar V R and Multani M 1995 *Phys. Rev. B* **52** 13177–83
- [28] Zhong W L, Wang Y G, Zhang P L and Qu B D 1994 *Phys. Rev. B* **50** 698–703
- [29] Shih W Y, Shih W H and Aksay I A 1994 *Phys. Rev. B* **50** 15575–85
- [30] Frey M H and Payne D A 1996 *Phys. Rev. B* **54** 3158–68
- [31] Debye P 1929 *Polar Molecules* reprint edn (New York: Dover)
- [32] Tagantsev A K 1994 *Phys. Rev. Lett.* **72** 1100–3
- [33] Sawyer C B and Tower C H 1930 *Phys. Rev.* **35** 0269–73
- [34] Mantas P Q 1999 *J. Eur. Ceram. Soc.* **19** 2079–86
- [35] Pelaiz-Barranco A, Garcia-Zaldivar O, Calderon-Pinar F, Lopez-Noda R and Betancourt J F 2005 *Phys. Status Solidi b* **242** 1864–7
- [36] Zhang L, Zhong W, Wang C, Peng Y and Wang Y 1999 *Eur. Phys. J. B* **11** 565–73
- [37] Zhang L, Zhong W, Wang C, Zhang P and Wang Y 1999 *J. Phys. D: Appl. Phys.* **32** 546–51

- [38] Zhang L, Zhong W, Wang C, Zhang P and Wang Y 1998 *Phys. Status Solidi a* **168** 543–8
- [39] Chen H, Yang C, Fu C, Zhao L and Gao Z 2006 *Appl. Surf. Sci.* **252** 4171–7
- [40] Tetsuka H, Takashima H, Prijamboedi B, Wang R P, Shoji A, Shan Y J and Itoh M 2006 *Phys. Status Solidi a* **203** 2546–50
- [41] Shaw T, Suo Z, Huang M, Liniger E, Laibowitz R and Baniecki J 1999 *Appl. Phys. Lett.* **75** 2129–31
- [42] Zhou L, Vilarinho P and Baptista J 1999 *J. Eur. Ceram. Soc.* **19** 2015–20
- [43] Fu H X and Bellaiche L 2003 *Phys. Rev. Lett.* **91** 257601
- [44] Naumov I I, Bellaiche L and Fu H X 2004 *Nature* **432** 737–40